Supplement of Hydrol. Earth Syst. Sci., 28, 1751–1769, 2024
https://doi.org/10.5194/hess-28-1751-2024-supplement

Hydrology and Earth System Sciences
Open Access

Supplement of

Influence of bank slope on sinuosity-driven hyporheic exchange flow and residence time distribution during a dynamic flood event

Yiming Li et al.

Correspondence to: Zhang Wen (wenz@cug.edu.cn)

This supporting information contains additional information on how the model used in our simulations was set up in COMSOL. We use the same methods, equations, and metrics described in Gomez-Velez et al. (2017), however, we implement here a deformed geometry method to capture the dynamic evolution of the wetting front along the sloping banks, while Gomez-Velez et al. (2017) assumed a vertical river bank. Due to their large file size, the COMSOL model files and the raw data to the figures in the manuscript are available upon request. For this please contact Yiming Li (liym@cug.edu.cn) or Zhang Wen (wenz@cug.edu.cn).

S1 Water flow model

The water flow model is based on that of Gomez-Velez et al. (2017), comprising an alluvial valley with a sinusoidal meandering river that overlies non-permeable river deposits, as shown in Fig. S1. To simplify the model, aquifer properties are assumed to be spatially homogeneous and isotropic. This means they can be modeled by the commonly used vertical-integrated approach which can reduce a 3-D groundwater flow problem to a two-dimensional (2-D) one, as shown in Fig. S2a. The model is bounded by hillslopes and a two-period fully penetrating sinusoidal river. By neglecting the compression of groundwater, unsteady, 2-D transient groundwater flow through the deformable aquifer is described by the Boussinesq's equation:

$$S_y \frac{\partial h}{\partial t} = \nabla[K(h - z_b)\nabla h] \tag{S1a}$$

$$h(\mathbf{x}, t = 0) = h_0(\mathbf{x}) \tag{S1b}$$

$$\mathbf{n} \cdot \nabla\, [K(h - z_b)\nabla h] = 0 \quad \text{for } \Omega_v \tag{S1c}$$

$$h(x_u, y, t) = h(x_d, y, t) + 2\,\lambda J_x \quad \text{for } \Omega_u \text{ and } \Omega_d \tag{S1d}$$

$$h(\mathbf{x}, t) = (\frac{J_x}{\sigma})s(x) + H_s(t) + 2\,\lambda J_x \quad \text{for } \Omega_{in} \cup \Omega_{out} \tag{S1e}$$

where $\mathbf{x} = (x, y)$ [L] is the spatial coordinate with x positive in the upstream direction, t [T] is simulation time, S_y [-] is specific yield, K [LT^{-1}] is the hydraulic conductivity, ∇ is the Laplace operator, $h(\mathbf{x}, t)$ and $h_0(\mathbf{x})$ [L] represent the hydraulic head at t and $t = 0$, while $z_b(\mathbf{x})$ [L] is the elevation of the underlying impermeable layer with respect to the reference datum $z = 0$ (see Fig. S2b and S2c), respectively. $H(\mathbf{x}, t) = h(\mathbf{x}, t) - z_b(\mathbf{x})$ [L] is the thickness of the saturated aquifer, $\mathbf{n}$ is the outward normal vector along the model boundary, Ω_v, Ω_u and Ω_d are the valley, upstream and downstream boundaries, respectively, while Ω_{in} and Ω_{out} are the inlet and outlet boundaries along the river. The fluxes are calculated by Darcy's law via $\mathbf{q} = -K\nabla h$ [LT^{-1}]. Here, $\mathbf{q}$ is the specific discharge or Darcy flux, $\mathbf{q}/\theta$ [LT^{-1}] is the pore water velocity with θ [-] as effective porosity, and $\mathbf{Q} = \mathbf{q}(h - z_b)$ [L^{2}T^{-1}] is the aquifer-integrated discharge in our 2-D model. The valley boundary (Ω_v) is assigned as a no-flow boundary and located at $y = n\lambda$, with the scaling number $n = 4.5$, which has proven to be sufficiently large for this simulation based on a series of pre-simulation tests while λ [L] is the wavelength of the river sinusoid. The river has been assigned a known transient hydraulic head, $h_r(x, t) = (J_x/\sigma)s(x) + H_r(t)$ [m], where J_x [-] is the base head gradient of ambient flow along the valley in positive x direction, $H_r(t)$ [L] is the elevation of river stage above the impermeable deposit at the downstream end.

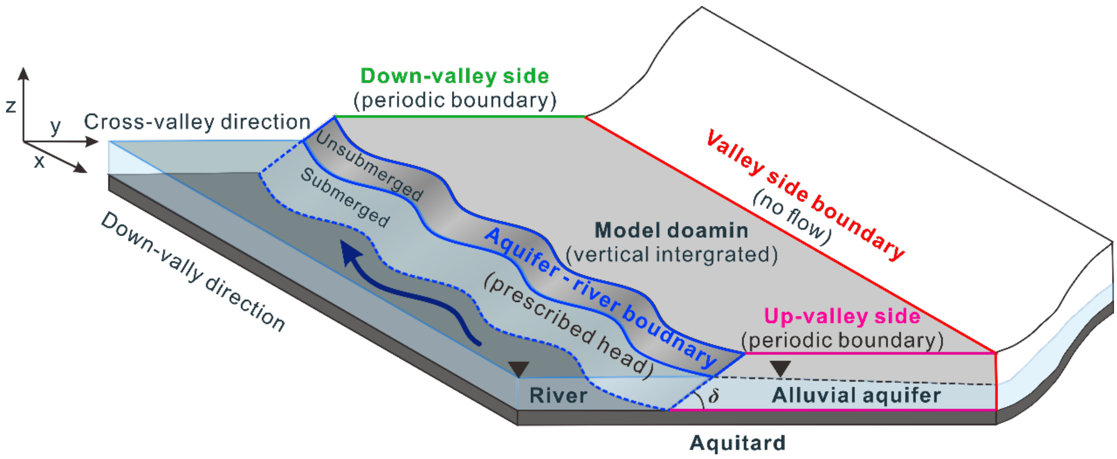

Figure S1. Conceptual model of the study area. Colored lines represent the river, up-valley, down-valley and valley side boundary conditions set in the model. Modified from Schmadel et al. (2016)

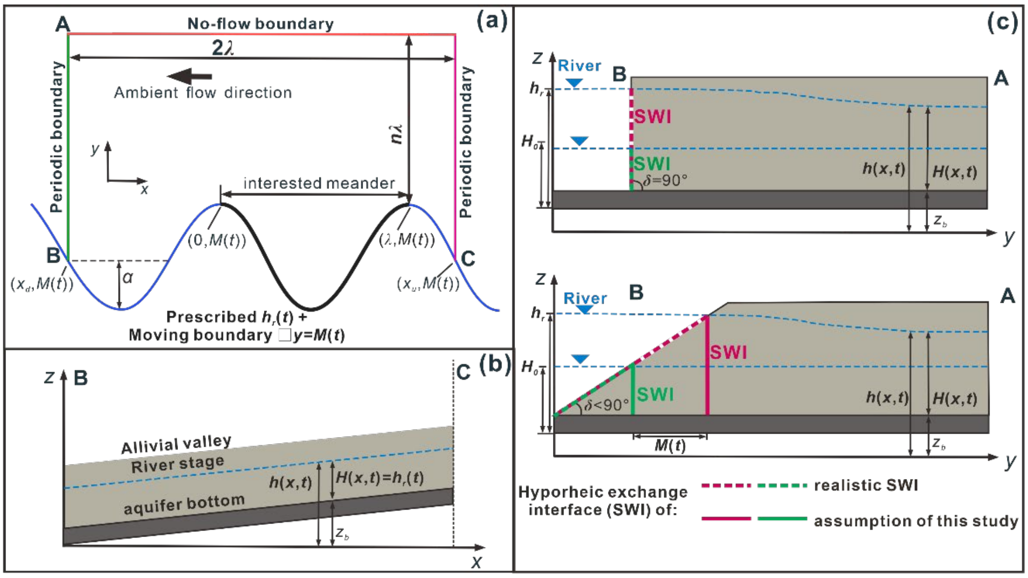

Figure S2. Modified after Gomez-Velez et al. (2017): (a) Schematic representation of the boundary conditions for the non-submerged alluvial system. The colors of the boundaries correspond to those in Fig. S1. (b) Representation of the stream stage variation along the channel thalweg. (c) Cross-section of unconfined aquifer and floodplain of vertical (δ = 90°) and sloping riverbank (δ < 90°). Green and red lines refer to the sediment-water interface (SWI) during base flow condition and flood event, respectively; the dashed lines on the riverbank surface and the vertical bold lines in Fig. S2c indicate the realistic SWIs and SWIs of this study, respectively.

The river ($\Omega_{in} \cup \Omega_{out}$) is implemented as a sinusoid, following the conceptualizations of Boano et al. (2006), Cardenas (2009a, 2009b), and Gomez-Velez et al. (2017). The initial condition is represented as: $y_0(x) = \alpha\cos(2\pi x/\lambda) - \alpha$, where α [L] is the amplitude of the river boundary. Left- and right-bottom vertices in initial condition are located at $x_d = -3\lambda/4$ and $x_u = 5\lambda/4$, respectively.

The impermeable bottom deposit $z_b = J_x(x - x_d)$ [L] is assumed to be parallel to the alluvial valley. Ω_u and Ω_d are periodic with a known variable hydraulic head drop $h(x = x_u, y, t) = h(x = x_d, y, t) + 2\lambda J_x$ [L] to eliminate any boundary effects. Thus, the model domain can represent two periodic parts in horizontal direction of the infinite aquifer. The river stage fluctuates during the dynamic flood event following (Cooper and Rorabaugh, 1963):

$$H_s = \begin{cases} H_0 + H_p \exp\left\{ -\eta(t-t_p)\dfrac{[1-\cos(wt)]}{[1-\cos(wt_p)]} \right\} & \text{if } 0 < t < t_p \\ H_0 & \text{if } t_p < t \end{cases} \qquad \text{(S2)}$$

where $H_0(\mathbf{x})$ [L] is the initial river stage, H_p [L] is the maximum (peak) river stage during the flood event, while t_d and t_p [T] are the duration of flood event and the time-to-peak river stage, respectively. $\omega = 2\pi/t_d$ [T^{-1}] is the flood event frequency, $\eta = \omega\cot(\omega t_p/2)$ [T^{-1}] represents the degree of flood event asymmetry. The peak river stage and time-to-peak are assumed to be linearly correlated with the base flow stage ($H_p = n_0 H_0$) and the duration of the event ($t_p = n_d t_d$), respectively. Constants n_0 [-] and n_d [-] represent river stage hydrograph intensity and skewness.

S2 Conservative solute transport model and calculation of HZ area (extent)

In this work, we adopt the mathematical model used by Gomez-Velez et al. (2017), where the transport of a conservative solute within the vertically integrated system is given by:

$$\frac{\partial(H\theta C)}{\partial t} = \nabla\cdot(\mathbf{D}\nabla C - \mathbf{Q}C) \qquad \text{(S3a)}$$

$$C(\mathbf{x}, t=0) = C_0(\mathbf{x}) \qquad \text{(S3b)}$$

$$\mathbf{n}\cdot(\mathbf{Q}C - \mathbf{D}\nabla C) = 0 \text{ for } \Omega_v \qquad \text{(S3c)}$$

$$C(x_u, y, t) = C(x_d, y, t) \text{ for } \Omega_u \text{ and } \Omega_d \qquad \text{(S3d)}$$

$$C(\mathbf{x}, t) = C_s(\mathbf{x}, t) \text{ for } \Omega_{in} \qquad \text{(S3e)}$$

$$\mathbf{n}\cdot(\mathbf{Q}C - \mathbf{D}\nabla C) = 0 \text{ for } \Omega_{out} \qquad \text{(S3f)}$$

where $C(\mathbf{x}, t)$, $C_0(\mathbf{x})$, and $C_S(\mathbf{x}, t)$ are the solute concentrations [ML^{-3}] in the aquifer, initial concentration and concentration in the river, respectively. The dispersion-diffusion tensor $\mathbf{D} = \{D_{ij}\}$ [L^2T^{-1}] is defined according to Bear and Cheng (2010) as:

$$D_{ij} = \alpha_T \left|\mathbf{Q}\right| \delta_{ij} + (\alpha_L - \alpha_T) \frac{Q_i Q_j}{\left|\mathbf{Q}\right|} + H\theta\epsilon\, D_L \tag{S4}$$

where α_T and α_L [L] are the transverse and longitudinal dispersivity, respectively, D_L [L^2T^{-1}] is the water diffusivity, $\epsilon = \theta^{1/3}$ [-] represents tortuosity (Millington and Quirk, 1961), and δ_{ij} [-] is the Kronecker delta function.

In order to mimic a periodical repetition of the meanders in x direction and eliminate potential boundary effects, a periodic boundary condition (Eq. (S3d)) is used at Ω_u and Ω_d. This type of boundary condition can produce the periodic nature of the model domain, flow field as well as the HZ that repeats for each meander bend (Gomez-Velez et al., 2017). However, in order to explore the local HZ that is caused by the HEFs at the studied meander: $0 < x < \lambda$ (i.e., bold black line along the meander in Fig. S2a), the conservative in-stream concentration is given by

$$C_s(t) = \begin{cases} 1 & \text{if } x \in [0, \lambda] \cap \Omega_{in} \\ 0 & \text{else} \end{cases} \tag{S5}$$

According to Eq. (S5), the river concentrations are assigned as an open boundary condition along the studied meander with the external concentration mimicking the concentration of the tracer (100% of stream water). Then the concentration of the pore water within the aquifer represents the fraction of water inflow from the river at any given location and time.

S3 Model of residence time distribution

The residence time (also terms as travel time or age) (RT) in the HZ describes the characteristic time scale over which water or solute molecule are exposed to the biogeochemical conditions within the hyporheic sediment. For HEF process, RT is controlled by the advective and dispersive characteristics of the system, thereby it is hard to calculate the RT of each molecule due extremely large computational demand. Thus, the residence time distribution equation was proposed (Ginn, 2000; Gomez-Velez et al., 2012,), and has been widely applied to calculate the mean residence time distribution (RTD) in HEF models (Gomez-Velez et al., 2017; Singh et al., 2019). Similar to Gomez-Velez et al. (2017), here we focus on the orders of moment of RTD that represent the mean residence time distribution:

$$\mu_n(\mathbf{x}, t) = \int_0^\infty \tau^n \rho(\mathbf{x}, t, \tau)\mathrm{d}\tau \qquad n = 0,\ 1,\ ... \tag{S6}$$

here, $\mu_n(\mathbf{x}, t)$ [T^n] is the n-th moment, $\rho(\mathbf{x}, t, \tau)$ [T^{-1}] is the residence time distribution, τ [T] is residence time, and $\mu_0 = 1$. The first moment of RTD ($\mu_r(\mathbf{x}, t)$) is the mean residence time distribution at a given location and time, which can be used to evaluate the transient variation of RTD. Here, we used the approach provided by Gomez-Velez et al. (2017) where the moments of RTD are calculated by a form of the advection-dispersion equation following

$$\frac{\partial(H\theta\mu_n)}{\partial t} = \nabla\cdot(\mathbf{D}\nabla\mu_n - \mathbf{Q}\mu_n) + nH\theta\mu_{n-1} \tag{S7a}$$

$$\mu_n(\mathbf{x}, t{=}0) = \mu_{n,0}(\mathbf{x}) \tag{S7b}$$

$$\mathbf{n}\cdot(\mathbf{Q}\mu_n - \mathbf{D}\nabla\mu_n) = 0 \text{ for } \Omega_v \tag{S7c}$$

$$\mu_n(x_u, y, t) = \mu_n(x_d, y, t) \text{ for } \Omega_u \text{ and } \Omega_d \tag{S7d}$$

$$\mu_n(\mathbf{x}, t) = 0 \text{ for } \Omega_{in} \tag{S7e}$$

$$\mathbf{n}\cdot(\mathbf{Q}\mu_n - \mathbf{D}\nabla\mu_n) = 0 \text{ for } \Omega_{out} \tag{S7f}$$

where $\mu_{n,0}(\mathbf{x}, t)$ is the initial condition of the n-th RTD that is calculated by the base flow condition (steady forcing before the arrival of flood event), while the upstream and downstream boundaries are assigned periodic boundary conditions (Eq. (S7d). As we ignore the vadose zone, the RT is defined as the time since the water entered the model domain from the river (i.e., the travel time of the water). Thus, n-th RTD at the inflow river boundary is zero (Eq. (S7e). A flow boundary is used for the region where the water exits the model domain (Eq. (S7f)).

S4 Validation of assumptions and using of DGM

The two main assumptions of this study are: (1) The SWI is always vertical and (2) the DGM can be used to represent the displacement of the SWI. In order to test the appropriateness of these assumptions, we built a 1-D horizontal model (from river channel to valley). Its flow field was calculated by the Boussinesq equation coupled with the DGM. We then built a 2-D vertical model (river channel to valley) the flow field of which was simulated by the Richard's equation. The diagrams of the 1-D and 2-D vertical models for validation are shown in Fig. S3a and Fig. S3b, respectively. Thus, the horizontal 1-D model (Fig. S3a) represents a reduced 2-D horizontal model (Fig. S2a, the model we use in our main manuscript) while the vertical 2-D model (Fig. 3b) represents a reduced 3-D model (described as Fig. S1), respectively. Our comparison neglects river sinuosity and the ambient groundwater flow gradient, but can efficiently prove the reliability of the vertical SWI assumption and usability of the DGM.

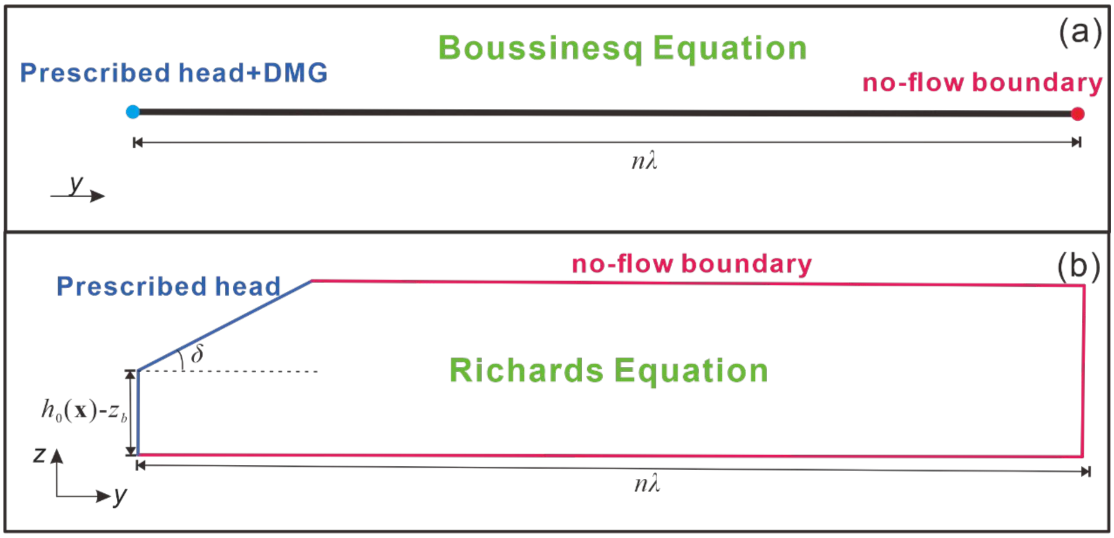

Figure S3. Diagrams of the 1-D horizontal and 2-D vertical model that we used to evaluate the appropriateness of the assumptions of this study. Blue lines and dot indicate the river boundary, red lines and dot indicate the no-flow boundary

The upper boundary of the 2-D model was higher than the peak river stage to avoid its submergence. The model length ($n\lambda$) has been shown to have no impact on the flow field (see S1), so the valley boundaries were set to be no-flow boundaries. The river boundary (SWI) of the 1-D model was assumed to be always vertical and the displacement of the SWI was calculated by Eq. (1) coupled with DGM. The model length and parameters were the same as shown in Table 1 in the main manuscript. The model mesh was refined near the river boundary with the total number of elements being 4168. The time step was 0.1 d with a total run time of 2*t_d.

For the vertical 2-D model corresponding to the 3-D model the flow field was simulated by the Richard's equation for unsaturated conditions which utilizes the van Genuchten equation for hydraulic properties (Van Genuchten, 1980):

$$k = KS_e^{0.5}\left[1-\left(1-S_e^{1/m}\right)^m\right]^2 \tag{S7a}$$

$$S_e = \left[1+\frac{1}{(\alpha\varphi)^n}\right]^m \tag{S7b}$$

$$S_e = \frac{S-S_r}{S_s-S_r} \tag{S7c}$$

$$m = 1-1/n \tag{S7d}$$

Here, k is hydraulic conductivity with specific saturation [LT^{-1}]; S is soil moisture content [-]; S_r is residual water content [-], which is assumed to be 0.01; S_s is saturated water content [-], which is equal to the porosity (0.3); S_e is the effective saturation [−]; α [L^{-1}] and n [-] are empirical coefficients, and assumed to be constant at 7.5 and 1.89, respectively while φ is pressure head [L]. The mesh was refined near the river boundary with a mesh size of 0.001 m, and a total number of mesh elements of 0.48 million. The total simulation time was 2*t_d with a time step of 0.1 d.

To evaluate the accuracy of our model approach for the scenarios tested in this study, the saturated hydraulic conductivity (parameterized by Γ_d) and bank slope angle were assigned to be the same as shown in Table 1 in the main manuscript. Fig. S4 shows the ratio of peak net flux of the 2-D to 1-D models ($R_p = Q^*_{max,2\text{-}D}/Q^*_{max,1\text{-}D}$). We could observe differences in net flux estimates between the 2-D vertical model (reduced 3-D) and the 1-D horizontal model even for vertical riverbank condition (δ = 90°), which resulted from the effect of the vadose zone (Liang et al., 2020). For sloping riverbank conditions these differences in net flux estimates remain albeit a change in magnitude.

Overall, the differences in peak net flux between horizontal 1-D and vertical 2-D models are mostly caused by the effect of the vadose zone. This implies that using the DGM has a minor influence on the prediction of the net flux in most of scenarios tested in this study.

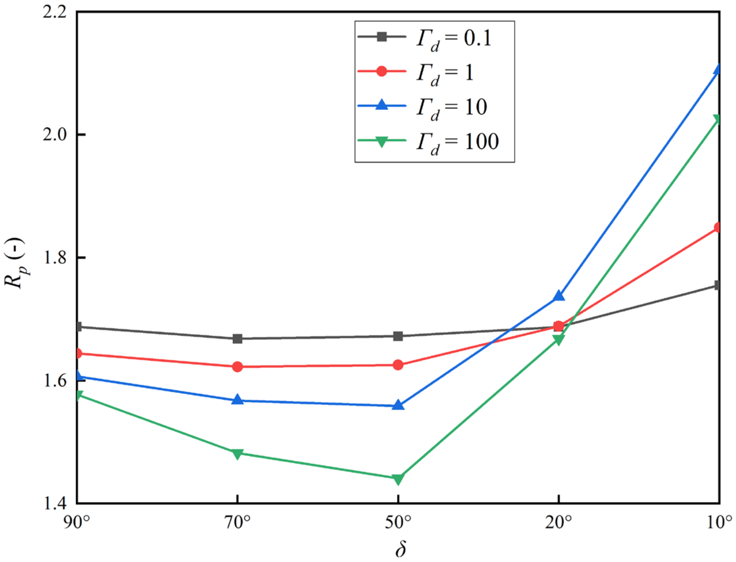

Figure S4. Ratio of maximum net flux of 2-D vertical model to 1-D horizontal model $R_p = Q^*_{max,2\text{-}D}/Q^*_{max,1\text{-}D}$ and aquifer transmissivities.

Figure S5 shows the relative difference in the bank storage between the 1-D horizontal and 2-D vertical model (R_s) for the scenarios tested in this study, which is calculated by:

$$R_s = \left(S_{2\text{-D}} - S_{1\text{-D}}\right) / S_{2\text{-D}} \tag{S8a}$$

$$S_{1\text{-D}} = \int h \mathrm{d}x \tag{S8b}$$

$$S_{2\text{-D}} = \iint \mathrm{d}x\mathrm{d}z \quad \text{if } S_e = 1 \tag{S8c}$$

where $S_{1\text{-D}}$ and $S_{2\text{-D}}$ are bank storage of 1-D and 2-D models [L^2], respectively. Fig. S5 indicates that the maximum difference in prediction of bank slope between 1-D and 2-D model were less than 15% under the condition with highest aquifer transmissivity (Γ_d = 0.1), however, the maximum R_p for $\Gamma_d = 0.1\delta = 90°$ was 11%, indicating the model approach of this study has minor influence on the model performance.

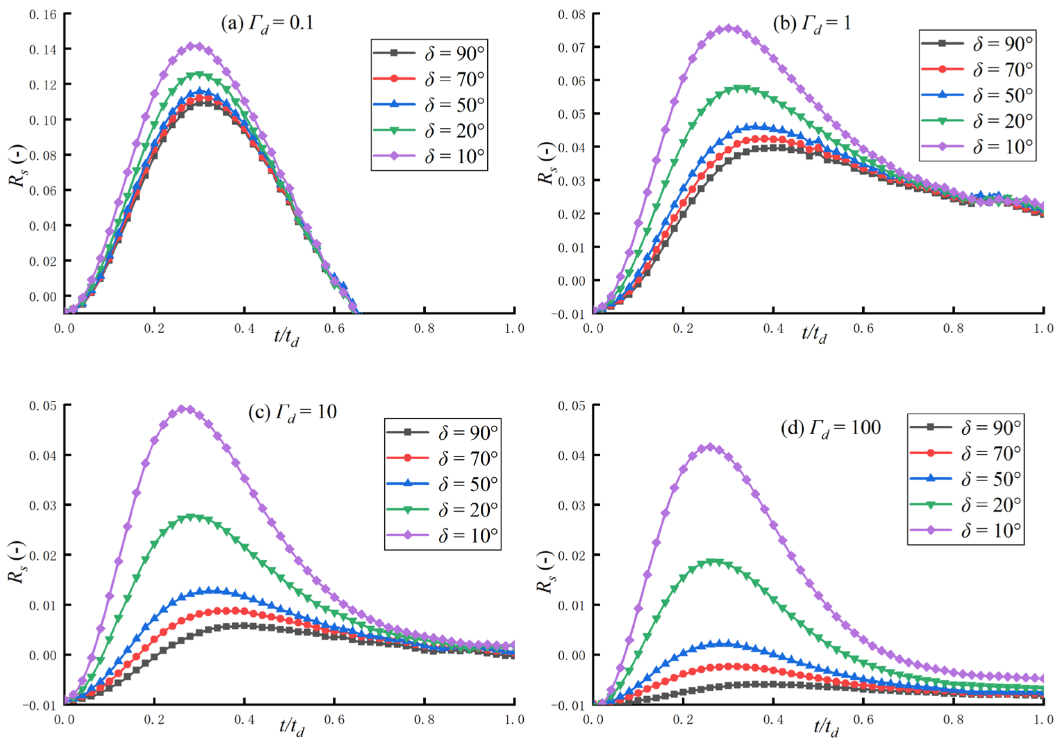

Figure S5. Relative difference in bank storage between vertical 2-D and horizontal 1-D model for various bank slope angle and aquifer transmissivity conditions.

While the using the Boussinesq equation neglects the influence of the vadose zone, this equation as well as the assumption of vertical integrated distribution of hydraulic head and solute have been widely used in the literature and proven adequate when simulating sinuosity-driven HEF patterns (Boano et al., 2006; 2010., Cardenas. 2008; 2009a, b; Gomez-Velez et al., 2012; 2017, Kruegler et al., 2020). Despite that, Fig. S4 and Fig. S5 show that differences in the prediction of HEF patterns exist between the Boussinesq model and Richard's model for all types of slope angle including a vertical riverbank indicating a discrepancy between both mathematical approaches. This discrepancy needs to be studied further to better understand the advantages and limitations of either approach, e.g., in terms of computability or efficiency in predicting HEF under various conditions.

S5 Metrics

We used the following dimensionless metrics to quantify the effects of bank slope angle on the response of the dynamic hyporheic zone: (i) hyporheic exchange flux along the river, (ii) in-valley penetration distance (i.e., the distance the river water penetrates into the aquifer), (iii) the area of the HZ (i.e., the area of the aquifer exposed to river water), and (iv) RTD and flux-weighted relative RT of HZ water discharging into the river. In this section, we briefly define and describe each of these terms.

S5.1 Hyporheic exchange flux

Exchange flux from the river to the HZ ($Q_{in,\,HZ}$) and from the aquifer to the river ($Q_{out,\,HZ}$) was defined as:

$$Q_{in,HZ}(t) = -\int_{\partial\Omega_{in,HZ}(t)} \mathbf{Q}(\mathbf{x},t)\cdot\mathbf{n}\,\mathrm{d}s \tag{S9a}$$

$$Q_{out,HZ}(t) = -\int_{\partial\Omega_{out,HZ}(t)} \mathbf{Q}(\mathbf{x},t)\cdot\mathbf{n}\,\mathrm{d}s \tag{S9b}$$

where $\Omega_{in,\,HZ}$ (t) and $\Omega_{out,\,HZ}$ (t) correspond to the inflow and outflow boundaries along the meander of interest (black line along the river boundary in Fig. S2a). The net flux from the aquifer into the river ($Q_{net,\,HZ} = Q_{out,\,HZ} - Q_{in,\,HZ}$) can be expressed in dimensionless terms following Gomez-Velez et al. (2017) using $Q^{*}_{in,\,HZ}(t) = Q_{in,\,HZ}(t)/(K\overline{H}_s^2)$, $Q^{*}_{out,\,HZ}(t) = Q_{out,\,HZ}(t)/(K\overline{H}_s^2)$, and $Q^{*}_{net,\,HZ}(t) = Q_{net,\,HZ}(t)/(K\overline{H}_s^2)$. Note that these dimensionless fluxes are proportional to the integrated head gradient between the river stage and the adjacent aquifer along the river boundary.

S5.2 Hyporheic zone area

Dynamic changes of the river-aquifer interface and pressure distribution along the SWI induce variations of the flow field and changes to the HZ as represented by area (i.e., the aquifer area exposed to river water) and penetration distance (i.e., how far river water travels into the aquifer) during the flood event. These are useful metrics for assessing the opportunity for biogeochemical and geochemical reactions induced by hyporheic exchange. Here we use a geochemical definition of HZ proposed by Triska et al. (1989), that defines the HZ as the area within the alluvial valley that contains more than 50% stream water ($C(\mathbf{x}, t) > 0.5$). It can be calculated using

$$A(t)=\iint a(\mathbf{x},t)\mathrm{d}x\mathrm{d}y \tag{S10a}$$

$$a(\mathbf{x},t)=\begin{cases} 1 & \text{if } C(\mathbf{x}, t) \geq 0.5 \\ 0 & \text{if } C(\mathbf{x}, t) < 0.5 \end{cases} \tag{S10b}$$

where $A(t)$ [L^2] is the area of the HZ. The dimensionless area is then defined similar to Gomez-Velez et al. (2017) as $A^*(t) = A(t)/\lambda^2$ and the dimensionless variation of the HZ area relative to base flow conditions can be calculated by $A^{**}(t) = A^*(t) - A^*(0)$, where $A^*(0)$ is the initial area of HZ under baseflow condition.

S5.3 Penetration distance of the hyporheic zone

The maximum penetration distance $d(t)$ of river water into the HZ in the direction perpendicular to the axis of the river can be calculated by the maximum y coordinate of the HZ. Similar to Gomez-Velez et al. (2017), we focus on the evolution of the dimensionless term of $d^{**}(t) = d^*(t) - d^*(0)$, where $d^*(t) = d(t)/\lambda$.

S5.4 Residence time

The difference in mean residence time distribution between a sloping and a vertical riverbank model was calculated by $\mu_r^*(\mathbf{x}, t) = \log_{10}(\mu_{\tau\text{-}S}(\mathbf{x}, t)/\mu_{\tau\text{-}V}(\mathbf{x}, 0)$. $\mu_r^* < 0$ indicating that RT was overestimated in these areas when ignoring the bank slope while $\mu_r^* > 0$ indicating the opposite. Furthermore, a representative value of the flux-weighted ratio of mean RT to mean RT under baseflow conditions along the river boundary is given by: $\mu^*_{\mathrm{out}}(x, t) = \mathbf{n}\cdot Q^*_{out}(x, \mathrm{t})\log_{10}(\mu_\tau(x, t)/\mu_\tau(x, 0))$, which indicates aquifer discharge of younger water with relatively short travel times (values smaller than zero) or older water with longer travel times within the alluvial aquifer as compared to the baseflow conditions.

References

Bear, J., and Cheng, A. H. D.: Modeling groundwater flow and contaminant transport, Vol. 23, P. 83, Dordrecht: Springer, https://doi.org/10.1007/978-1-4020-6682-5, 2010.

Boano, F., Camporeale, C., Revelli, R., and Ridolfi, L.: Sinuosity-driven hyporheic exchange in meandering rivers, Geophys. Res, Lett., 33, L18406, https://doi.org/10.1029/2006GL027630, 2006.

Boano, F., Demaria, A., Revelli, R., and Ridolfi, L.: Biogeochemical zonation due to intrameander hyporheic flow, Water Resour. Res., 46, W02511, https://doi.org/10.1029/2008WR007583, 2010.

Cardenas, M. B.: A model for lateral hyporheic flow based on valley slope and channel sinuosity, Water Resour. Res., 45, W01501, https://doi.org/10.1029/2008WR007442, 2009a.

Cardenas, M. B.: Stream-aquifer interactions and hyporheic exchange in gaining and losing sinuous streams, Water Resour. Res., 45, W06429, https://doi.org/10.1029/2008WR007651, 2009b.

Cardenas, M. B.: The effect of river bend morphology on flow and timescales of surface water-groundwater exchange across pointbars, J. Hydrol., 362, 134-141, https://doi.org/10.1016/j.jhydrol.2008.08.018, 2008.

Cooper, H. H., and Rorabaugh, M. I.: Ground-water movements and bank storage due to flood stages in surface streams, Report of Geological Survey Water-Supply, P. 1536-J, US Government Printing Office, Washington, United States, 1963.

Ginn, T. R.: On the distribution of multicomponent mixtures over generalized exposure time in subsurface flow and reactive transport: Foundations, and formulations for groundwater age, chemical heterogeneity, and biodegradation. Water Resour. Res., 35(5), 1395-1407, https://doi.org/10.1029/1999WR900013, 1999.

Gomez-Velez, J. D., and Harvey, J. W.: A hydrogeomorphic river network model predicts where and why hyporheic exchange is important in large basins, Geophys.

Res. Lett., 41, 6403–6412, https://doi.org/10.1002/2014GL061099, 2014.

Gomez, J. D., J. L. Wilson, and M. B. Cardenas.: Residence time distributions in sinuosity-driven hyporheic zones and their biogeochemical effects, Water Resour. Res., 48, W09533, https://doi.org/10.1029/2012WR012180, 2012.

Gomez-Velez, J. D., Wilson, J. L., Cardenas, M. B., and Harvey, J. W.: Flow and residence times of dynamic river bank storage and sinuosity-driven hyporheic exchange, Water Resour. Res., 53, 8572-8595, https://doi.org/10.1002/2017WR021362, 2017.

Kruegler, J., Gomez-Velez, J. D., Lautz, L. K., and Endreny, T. A.: Dynamic evapotranspiration alters hyporheic flow and residence times in the intrameander zone, Water, 12 (2), 424, https://doi.org/10.3390/w12020424, 2020.

Liang, X. Y., Zhan, H. B., and Schilling, K.: Spatiotemporal responses of groundwater flow and aquifer-river exchanges to flood events, Water Resour. Res., 54 (3), 1513-1532, https://doi.org/10.1002/2017WR022046, 2018.

Millington, R. J., and Quirk, J. P.: Permeability of porous solids, Transactions of the Faraday Society, 57, 1200-1207, 1961.

Schmadel, N. M., A. S. Ward, C. S. Lowry, and J, M. Malzone.: Hyporheic exchange controlled by dynamic hydrologic boundary conditions, Geophys. Res. Lett., 43, 4408-4417, https://doi.org/10.1002/2016GL068286, 2016.

Singh, T., Wu, L., Gomez-Velez, J. D., Lewandowski, J., Hannah, D. M., and Krause, S.: Dynamic hyporheic zones: Exploring the role of peak flow events on bedform-induced hyporheic exchange, Water Resour. Res., 55, 218–235, https://doi.org/10.1029/2018WR022993, 2019.

Triska, F. J., Kennedy, V. C., Avanzino, R. J., Zellweger, G. W., & Bencala, K. E.: Retention and transport of nutrients in a third-order stream in northwest California: Hyporheic processes, Ecology, 70 (6), 1893-1905, https://doi.org/10.2307/1938120, 1989.

Van Genuchten, M. T.: A closed - form equation for predicting the hydraulic conductivity of unsaturated soils. Soil sci. soc. Am. J., 44(5), 892-898, https://doi.org/10.2136/sssaj1980.03615995004400050002x, 1980.